Computational Mechanics 20 (1997) 26–33 © Springer-Verlag 1997

Symmetric Galerkin boundary integral fracture analysis for plane orthotropic elasticity

L. J. Gray, G. H. Paulino

Abstract This paper discusses the formulation and implementation of the symmetric Galerkin boundary integral method for two dimensional linear elastic orthotropic fracture analysis. For the usual case of a traction-free crack, the symmetry of the coefficient matrix can be effectively exploited to significantly reduce the computational work required to construct the linear system. In addition, computation time is reduced by employing efficient analytic integration formulas for the analysis of the orthotropic singular and hypersingular integrals. Preliminary test calculations indicate that the method is both accurate and efficient.

1 Introduction

Numerical methods such as finite elements and boundary elements are essential for solving engineering fracture mechanics problems. A disadvantage of the finite element method is the need to discretize the entire volume around the crack. This makes simulation of crack propagation a very dificult task, especially in three-dimensions and for multiple crack problems. The boundary element method (BEM) permits an elegant treatment of the fracture problem, although efficient crack modeling has proven to be a challenging task.

The direct application of the standard boundary integral equation (BIE) for discrete cracks is known to be an ill-posed problem (Cruse 1988). Special Green's functions for a traction-free crack of simple geometry (straight or an arc of a circle) have been developed (e.g. Paulino, Saif and Mukherjee 1993), but these techniques are generally based on complex variables and are therefore limited to two-dimensional (2D) problems. Moreover, the BIE treatment of multiple crack problems by means of conformal mapping and complex variables is quite complicated.

The multi-domain formulation of Blandford, Ingraffea and Liggett (1981) is a general purpose boundary integral fracture algorithm. The method consists of dividing the domain into zones such that the cracks lie along the zone boundaries, and hence no crack appears in the interior of any zone. In this process, interior nodes and elements are introduced to connect the crack(s) to the outer boundary. Tan and Gao (1992) have applied this technique to orthotropic elasticity. The two main disadvantages of the multi-domain method are the computational expense and the necessity of dealing with the singular stress field ahead of the crack. Both of these negative aspects are due to the introduction of 'artificial separation surfaces'. In addition, these surfaces also make this method impractical for an automatic crack propagation simulation.

The field of hypersingular boundary integral equations (HBIEs) has opened possibilities for new solutions of various problems by the BEM (see, for example, the review article by Krishnasami et al. 1992). Recently, methods based on HBIEs have been developed to overcome the problems inherent in the multi-domain method. There are a number of hypersingular approaches, and each approach has been developed independently by several groups, see for example Bonnet and Bui (1993); Cruse (1988); Chang and Mear (1995); Gray, Martha and Ingraffea (1990); Guimarães and Telles (1994); Hong and Chen (1988); Paulino (1995); Selcuk et al. (1994). Although successful, the common problem for these methods is that, when employed in conjunction with a *collocation* approximation, a smoothness constraint is necessarily imposed on the boundary displacement (Gray 1991; Martin and Rizzo 1996). This differentiability condition adds considerable complexity to the fracture algorithm. Higher order differentiable interpolations, such as Overhauser elements (Walters et al. 1988; Hall and Hibbs 1988) or Hermite elements (Watson 1986; Rudolphi 1990) are difficult to work with and are computationally expensive. An alternative is to avoid the differentiability issue by using non-conforming elements, i.e. collocating[1] interior to the element instead of at the endpoints (e.g. Selcuk et al. 1994). However, this adds significantly to the number of unknowns, especially in three-dimensions, and is therefore also quite expensive.

L. J. Gray
Computer Science and Mathematics Division, Oak Ridge National Laboratory, Oak Ridge, TN 37831-6367, USA

G. H. Paulino
Department of Civil and Environmental Engineering, University of California, Davis, CA 95616-5294, USA

Correspondence to: L. J. Gray

This research was partially supported by the Applied Mathematical Sciences Research Program of the Office of Mathematical, Information, and Computational Sciences, U.S. Department of Energy under contract DE-AC05-96OR22464 with Lockheed Martin Energy Research Corp. L. J. Gray would like to thank Prof. M. R. Ramey for hospitality at UC-Davis. G. H. Paulino acknowledges the "1995-96" New Faculty Research Grant" from the UC-Davis Academic Senate. The authors appreciate the help of Dr. P. A. Wawrzynek with the FEM program FRANC.

[1] To collocate interior to the element means to enforce the respective HBIE at one or more interior points of the element.

In this paper, further development of the symmetric Galerkin (SG) boundary integral method (Hartman et al. 1985; Maier and Polizzoto 1987; Sirtori et al. 1992) for fracture mechanics problems is presented. The *Galerkin* approximation allows the use of standard continuous elements, while the *symmetric* implementation reduces the computational cost to that of collocation methods. This work focuses on discrete crack modeling applied to plane orthotropic elastic problems. The hypersingular formulation for orthotropic solids is introduced here, and techniques for improving the efficiency of the SG fracture algorithm are presented.

The remaining sections of this paper are organized as follows. First, the governing equations for the symmetric Galerkin analysis, considering orthotropic elasticity, are presented. Second, the fracture algorithm is discussed, which includes the appropriate selection of the crack variables, and issues concerning the computational efficiency of the algorithm. Next, the evaluation of singular integrals is described with emphasis on the isolation and cancellation of potentially singular terms. Afterwards, example calculations are presented. The paper concludes with a few remarks, followed by a discussion of directions for future research. The Appendix presents the formulas for the kernel functions in the HBIE.

2
Symmetric Galerkin BEM

The basic SG framework for 2D orthotropic elastic boundary value problems is introduced in this section. Since the SG method employs both the BIE and the HBIE, these equations are discussed first. The mathematical formulation is developed, and some numerical issues are presented. The actual fracture algorithm is developed in the next section.

2.1
Orthotropic boundary integral equations

In order to present the hypersingular traction equation we briefly review the boundary integral formulation for two dimensional orthotropic elasticity presented by Rizzo and Shippy (1970). As usual, let u_j and σ_{jk} denote the components of the displacements and stresses. For plane stress, the stress-strain relationship is given by

$$\begin{aligned}\sigma_{11} &= c_{11}u_{1,1} + c_{12}u_{2,2}\\ \sigma_{22} &= c_{12}u_{1,1} + c_{22}u_{2,2}\\ \sigma_{12} &= c_{66}(u_{1,2} + u_{2,1}) \ ,\end{aligned} \tag{1}$$

where c_{ij} are material constants (stiffnesses), and $(\cdot)_{,i} = \partial(\cdot)/\partial x_i$. Moreover, the Navier-Cauchy equilibrium equations, in the absence of body forces, are

$$\begin{aligned}c_{11}u_{1,11} + (c_{12} + c_{66})u_{2,12} + c_{66}u_{1,22} &= 0\\ c_{22}u_{2,22} + (c_{12} + c_{66})u_{1,12} + c_{66}u_{2,11} &= 0 \ .\end{aligned} \tag{2}$$

The BIE for anisotropic elasticity has the same form as for the isotropic case, the difference being the fundamental solution. Thus, the BIE takes the usual form

$$u_k(P) = \int_\Gamma U_{kj}(P,Q)\tau_j(Q)\mathrm{d}Q - \int_\Gamma T_{kj}(P,Q)u_j(Q)\mathrm{d}Q \ , \tag{3}$$

where $u_k(Q)$ and $\tau_k(Q)$ are the boundary displacement and traction vectors, respectively, and $U_{kj}(P,Q)$ is the fundamental solution, i.e. the displacement field at Q due to a point force at P in an infinite sheet of orthotropic material (Green 1943; Rizzo and Shippy 1970). This function, in component form, is given by

$$\begin{aligned}U_{11}(P,Q) &= \frac{1}{\beta}\left[\sqrt{\alpha_1}A_2^2\log(r_1) - \sqrt{\alpha_2}A_1^2\log(r_2)\right]\\ U_{12}(P,Q) &= \frac{1}{\beta}\left[A_1A_2(\theta_2 - \theta_1)\right]\\ U_{21}(P,Q) &= U_{12}(P,Q)\\ U_{22}(P,Q) &= \frac{1}{\beta}\left[\frac{A_2^2\log(r_2)}{\sqrt{\alpha_2}} - \frac{A_1^2\log(r_1)}{\sqrt{\alpha_1}}\right] \ ,\end{aligned} \tag{4}$$

where the constants are defined by $\beta \equiv 2\pi(\alpha_1 - \alpha_2)/s_{22}$, $A_k = s_{12} - \alpha_k s_{22}$, $\alpha_1 + \alpha_2 = (2s_{12} + s_{66})/s_{22}$, and $\alpha_1\alpha_2 = s_{11}/s_{22}$. Moreover

$$\begin{bmatrix} c_{11} & c_{12}\\ c_{12} & c_{22}\end{bmatrix} = \begin{bmatrix} s_{11} & s_{12}\\ s_{12} & s_{22}\end{bmatrix}^{-1} \quad \text{and} \quad c_{66} = \frac{1}{s_{66}} \ . \tag{5}$$

The distance and angle functions are defined by

$$r_k^2 = (Q_1 - P_1)^2 + \frac{1}{\alpha_k}(Q_2 - P_2)^2 \tag{6}$$

and

$$\theta_k = \tan^{-1}\left[\frac{Q_2 - P_2}{\sqrt{\alpha_k}(Q_1 - P_1)}\right] \ , \tag{7}$$

respectively, where the coefficients α_k are assumed to be real and positive. The traction fundamental solution $T_{kj}(P,Q)$, in component form, is

$$\begin{aligned}T_{11}(P,Q) &= \frac{1}{\beta}\mathbf{n}\cdot\mathbf{R}\left(\frac{A_1}{\sqrt{\alpha_2}r_2^2} - \frac{A_2}{\sqrt{\alpha_1}r_1^2}\right)\\ T_{12}(P,Q) &= \frac{1}{\beta}\left(\frac{M_1A_2}{r_1^2} - \frac{M_2A_1}{r_2^2}\right)\\ T_{21}(P,Q) &= \frac{1}{\beta}\left(\frac{M_1A_1}{\alpha_1r_1^2} - \frac{M_2A_2}{\alpha_2r_2^2}\right)\\ T_{22}(P,Q) &= \frac{1}{\beta}\mathbf{n}\cdot\mathbf{R}\left(\frac{A_1}{\sqrt{\alpha_1}r_1^2} - \frac{A_2}{\sqrt{\alpha_2}r_2^2}\right)\end{aligned} \tag{8}$$

where $\mathbf{R} = Q - P$ and $\mathbf{n} = \mathbf{n}(Q)$ is the unit normal vector at Q. The parameter M_k is

$$M_k = \sqrt{\alpha_k}n_y(Q_1 - P_1) - \frac{n_x}{\sqrt{\alpha_k}}(Q_2 - P_2) \ . \tag{9}$$

For a point P interior to the domain, the displacement Eq. (3) can be differentiated with respect to P, the derivative moved underneath the integral sign, resulting in

$$u_{k,L}(P) \equiv \int_\Gamma S_{kjL}(P,Q)\tau_j(Q)\mathrm{d}Q - \int_\Gamma W_{kjL}(P,Q)u_j(Q)\mathrm{d}Q \ , \quad (10)$$

where

$$S_{kjL} = U_{kj,L} \quad \text{and} \quad W_{kjL} = T_{kj,L} \ . \quad (11)$$

The formulas for the kernel functions S_{kjL} and W_{kjL} are somewhat lengthy and can be found in the Appendix. The desired integral equation for surface traction can now be formed by combining the equations for displacement derivatives according to Eq. (1),

$$\tau_k(P) = \int_\Gamma \hat{S}_{kj}(P,Q)\tau_j(Q)\mathrm{d}Q - \int_\Gamma \hat{W}_{kj}(P,Q)u_j(Q)\mathrm{d}Q \ , \quad (12)$$

where $\hat{S}_{kj}$ and $\hat{W}_{kj}$ are appropriate linear combinations of S_{kjL} and W_{kjL}, respectively. As indicated above, this equation is strictly valid for an interior point P. However, it can be shown that the limit as P approaches the boundary exists, and thus for $P \in \Gamma$, the traction equation is understood in this limiting sense. The boundary integral equations are usually written with a geometry-dependent coefficient multiplying the displacement and traction functions outside the integrals. In the above formulation, this coefficient has been absorbed into the integrals, appearing automatically when the *limit to the boundary* evaluation is carried out (Lutz and Gray 1993; Paulino 1995). Aside from avoiding potential difficulties in evaluating this coefficient (Rizzo et al. 1985), this approach allows a unified and direct treatment of the singular integrals appearing in both the BIE (3) and the HBIE (12), and these equations remain valid for both interior and boundary points!

2.2 Basic symmetric Galerkin procedure

The key to obtaining a symmetric coefficient matrix are the symmetry property of the kernel functions ($\mathbf{U}, \mathbf{T}, \hat{\mathbf{W}}$ and $\hat{\mathbf{S}}$), combined with a Galerkin approximation. Galerkin differs from collocation in that Eqs. (3) and (12) are satisfied in an averaged sense, rather than at individual points. Specifically, the weighting functions are chosen to be the basis shape functions ψ_l (e.g. linear: $\{l = 1, 2\}$; quadratic: $\{l = 1, 2, 3\}$) employed in the approximation of displacement and traction on the boundary. Thus, the form of the displacement equation to be solved numerically is

$$\int_\Gamma \psi_l(P)u_k(P)dP + \int_\Gamma \psi_1(P)\int_\Gamma T_{kj}(P,Q)\,u_j(Q)\mathrm{d}Q\ \mathrm{d}P - \int_\Gamma \psi_l(P)\int_\Gamma U_{kj}(P,Q)\,\tau_j(Q)\mathrm{d}Q\ dP = 0 \ , \quad (13)$$

and similarly for the traction equation,

$$\int_\Gamma \psi_l(P)\tau_k(P)dP + \int_\Gamma \psi_l(P)\int_\Gamma \hat{W}_{kj}(P,Q)\,u_j(Q)\mathrm{d}Q\ \mathrm{d}P - \int_\Gamma \psi_l(P)\int_\Gamma \hat{S}_{kj}(P,Q)\,\tau_j(Q)\mathrm{d}Q\ \mathrm{d}P = 0 \ . \quad (14)$$

The additional boundary integration is required to obtain a symmetric matrix, as this ensures that the source P and the field Q are treated on the same fashion. The last component of the SG formulation is the choice of equation–the displacement BIE (13) is employed on the surface with prescribed displacements ($\Gamma_\mathbf{u}$), and the traction BIE (14) is employed on the surface with prescribed tractions (Γ_τ). Note that for a well posed boundary value problem $\Gamma = \Gamma_\mathbf{u} + \Gamma_\tau$.

After discretization, the resulting set of equations in matrix form can be written as

$$[\mathscr{H}]\{u\} = [\mathscr{G}]\{\tau\} \ , \quad (15)$$

and in block matrix notation, these equations take the form

$$\begin{bmatrix} H_{11} & H_{12} \\ H_{21} & H_{22} \end{bmatrix} \begin{Bmatrix} u_{bv} \\ u_* \end{Bmatrix} = \begin{bmatrix} G_{11} & G_{12} \\ G_{21} & G_{22} \end{bmatrix} \begin{Bmatrix} \tau_* \\ \tau_{bv} \end{Bmatrix} \ . \quad (16)$$

The first row represents the BIE written on the $\Gamma_\mathbf{u}$ surface, and the second represents the HBIE on the Γ_τ surface. Similarly the first and second columns arise from integrating over $\Gamma_\mathbf{u}$ and Γ_τ surfaces. The subscripts in the vectors denote known boundary values (bv) and unknown (*) quantities. Rearranging Eq. (16) into the form $[A]\{x\} = \{b\}$, and multiplying the hypersingular equations by -1, one obtains

$$\begin{bmatrix} -G_{11} & H_{12} \\ G_{21} & H_{22} \end{bmatrix} \begin{Bmatrix} \tau_* \\ u_* \end{Bmatrix} = \begin{Bmatrix} -H_{11}\,u_{bv} + G_{12}\,\tau_{bv} \\ H_{21}\,u_{bv} - G_{22}\,\tau_{bv} \end{Bmatrix} \ . \quad (17)$$

The symmetry of the coefficient matrix, $G_{11} = G_{11}^T$, $H_{22} = H_{22}^T$, and $H_{12} = G_{21}^T$, now follows from the symmetry properties of the kernel functions.

3 Symmetric Galerkin fracture analysis

A Symmetric Galerkin algorithm for fracture, in the context of two-dimensional potential theory, has recently been presented by Gray et al. (1995). This method, effectively a combination of the displacement discontinuity (Crouch and Starfield 1983) and the dual BIE (e.g. Gray et al. 1990) ideas, employs the hypersingular equation on the crack surface to solve for the jump in displacement across the fracture. Our goal herein is to discuss techniques for improving the computational efficiency of this approach, so we first provide a brief review of this method. Moreover, in this work, the crack modelling approach is extended to plane orthotropic elasticity.

Consider a 2D linear elastic orthotropic body which contains a crack, as illustrated by Fig. 1. In the dual equation boundary integral method, independent equations for solving for the crack displacements on both sides are obtained by writing both standard and hypersingular equations on the crack surfaces. This violates the symmetric-Galerkin procedure, as the boundary condition is invariably specified traction and consequently only the traction equation should be used. Symmetry of the coefficient matrix is therefore not possible with the dual equation method. Nevertheless, taking this approach as a starting point for a symmetric-Galerkin fracture formulation, the resulting system of equations can be written in the block-matrix form

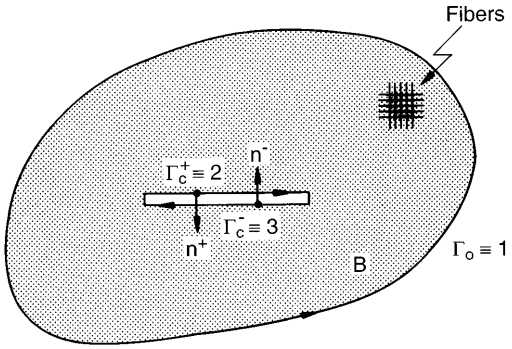

Fig. 1. A body B with a crack. The body has boundary $\Gamma = \Gamma_o + \Gamma_c$. Moreover, $\Gamma_o = \Gamma_{o(u)} + \Gamma_{o(\tau)}$ and $\Gamma_c = \Gamma_c^+ + \Gamma_c^-$

$$\left[\begin{array}{cc|c} h_{11} & h_{12} & h_{13} \\ h_{21} & h_{22} & h_{23} \\ \hline h_{31} & h_{32} & h_{33} \end{array}\right] \left\{\begin{array}{c} \Omega_1 \\ u_2 \\ \hline u_3 \end{array}\right\} = \left[\begin{array}{cc|c} g_{11} & g_{12} & g_{13} \\ g_{21} & g_{22} & g_{23} \\ \hline g_{31} & g_{32} & g_{33} \end{array}\right] \left\{\begin{array}{c} \hat{\Omega}_1 \\ \tau_2 \\ \hline \tau_3 \end{array}\right\} \quad . \tag{18}$$

The blocking strategy, according to Fig. 1, is as follows: the first row and column is associated with the outer, non-crack boundary Γ_O, while the subscripts 2 and 3 refer to the two sides of the crack Γ_c^+ and Γ_c^-, respectively. The vector of unknowns on the outer boundary (Γ_O) is in general a mixture of displacement and traction, and is denoted by Ω_1. The corresponding vector of prescribed boundary values is indicated by $\hat{\Omega}_1$. The second and third rows correspond to the equations for traction and displacement, respectively, written on the crack surface. It is assumed that the traction is specified on the crack surfaces.

Note that although the coefficient matrix in Eq. (18) is not symmetric, the upper 2×2 principal submatrix is, i.e. $h_{11} = h_{11}^T, h_{22} = h_{22}^T$, and $h_{21} = h_{12}^T$. This is a consequence of the basic SG procedure, the traction equation being the appropriate choice on the fracture. In addition to the symmetry, it is also important to observe that $h_{13} = -h_{12}$ and $h_{23} = -h_{22}$, a consequence of the change in surface orientation in the (nonsingular) integration over the two sides of the fracture. It can be shown that a symmetric coefficient matrix results from changing variables on the crack from displacement to jump in displacement (i.e. displacement discontinuity Δu),

$$\Delta u = u_2 - u_3, \quad \Sigma u = u_2 + u_3 \quad . \tag{19}$$

With this transformation, the left hand side of Eq. (18) takes the form

$$\left[\begin{array}{cc|c} h_{11} & h_{12} & 0 \\ h_{12}^T & h_{22} & 0 \\ \hline h_{31} & h_{32} & I/2 \end{array}\right] \left\{\begin{array}{c} \Omega_1 \\ \Delta u \\ \hline \Sigma u \end{array}\right\} \quad , \tag{20}$$

where I is the identity matrix. It therefore suffices to solve the smaller *symmetric* 2×2 block system for the unknowns $\{\Omega_1, \Delta u\}$. If necessary, Σu, and hence the displacements u_2 and u_3 on the crack surfaces (see Fig. 1), can be calculated in a post-processing step after $\{\Omega_1, \Delta u\}$ have been determined. To this effect, the construction of the matrices h_{31} and h_{32} is needed, however, no linear solution is required, as the coefficient matrix of Σu is the identity.

4
Singular integrals

A key part of any boundary integral algorithm is the evaluation of singular integrals. The present SG implementation differs in two aspects from those reported in the literature, and thus these issues are discussed below. We first present a slightly different boundary limit process for performing the integrations when the P and Q elements coincide, i.e. the coincident singular integrations. This modification is specific to the orthotropic Green's function, but the second item, the isolation of potentially singular terms should be generally applicable for SG analysis. The goal will be to provide enough information to describe the new algorithms, almost all of the details will be omitted. In addition, the discussion of the limit process will be confined to the hypersingular integral in Eq. (12), i.e. the integral with kernel $\hat{\mathbf{W}}$. The analysis of the remaining integrals is simpler and follows in a similar fashion.

It suffices to assume a linear element,

$$Q(s) = (1-s)Q_l + sQ_m, \quad s \in [0,1] \quad , \tag{21}$$

interpolating the neighboring boundary nodes Q_l and Q_m. Singular integrals arising from higher order curved elements can eventually be reduced to the same form as linear element integrals (Gray 1993; Paulino 1995) and thus the same techniques apply.

4.1
Boundary limit

The Galerkin formulation (see Eqs. (13) and (14)) requires integration over a pair of elements, the outer P and inner Q integrals. For a given P element $E_P = E_0$, singular integrals arise when the Q integration is *coincident*, namely $E_Q = E_P$, or when the E_Q element is one of the two *adjacent* elements E_{-1} or E_1. This is illustrated in Fig. 2. The *limit to the boundary* procedure is only required to define the coincident integrals.

Referring to the Appendix, one verifies that the hypersingular kernel consists of linear combinations of functions of the form

$$\mathscr{F}(P,Q) = \frac{(Q_m - P_m)(Q_l - P_l)}{r_k^4} \quad , \tag{22}$$

where $k, m, l = 1, 2$. If a line integral of this function includes $P = Q$, the integral can be defined by first moving the point P off the boundary in the direction $\boldsymbol{L}$, i.e.

$$P \to P - \varepsilon \boldsymbol{L}, \quad \|L\| = 1 \quad , \tag{23}$$

evaluating the integral, and then taking the limit $\varepsilon \to 0$. The usual procedure is to move P *normal* to the boundary, i.e. $\boldsymbol{L} = (n_x, n_y)$, as this results in the simplest integration. For the orthotropic Green's function however, the distance

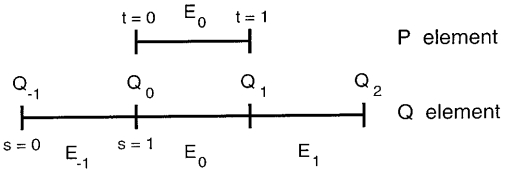

Fig. 2. Illustration of the coincident ($E_Q = E_P = E_0$) and adjacent (e.g. $E_P = E_0, E_Q = E_{-1}$) singular integrations

function in the denominator is weighted in the y component,

$$r_k = \left[(Q_1 - P_1)^2 + \frac{(Q_2 - P_2)^2}{\alpha_k} \right]^{\frac{1}{2}} , \tag{24}$$

and in this case a normal limit direction is not optimal. By choosing the approach direction $\boldsymbol{L} = (n_x, \alpha n_y)$, r_k takes the form

$$r_k = \left[b_2 (s - t)^2 + b_0 \varepsilon^2 \right]^{\frac{1}{2}} , \tag{25}$$

where s and t are the parameters for the Q and P integrations, respectively. The advantage of this compared to a normal limit is that there is no linear term $b_1(s - t)$, and this considerably simplifies the resulting integration formulas. This simplicity translates into less computational effort in evaluating the integrals.

Note that for a collocation approximation, singular integral computation time is not a major issue. The analogous singular integrals are only evaluated once for each node, and thus the total computational expense is relatively minor. In a Galerkin approximation, however, the additional integration with respect to P means that these formulas are executed for each Gauss point in the outer (numerical) quadrature. Maximizing the efficiency of the integration formulas is therefore more critical.

4.2
Cancelling of singularities

Consider the adjacent singular integration with $E_P = E_0$, $E_Q = E_{-1}$, the singularity occurring when $P = Q = Q_0$, as shown in Fig. 2. In evaluating this integral, it would be convenient to replace the parameters $\{s, t\}$ with polar coordinates $\{\rho, \theta\}$ centered at Q_0. This is desirable because the troublesome part of the integral is at $\rho = 0$, and the ρ integration can be performed analytically. However, this is not entirely possible, for the following reason.

The hypersingular integral is well defined because the boundary limit exists, independent of limit direction. However, potentially singular terms, which eventually cancel, do arise in the integration, and it is important to ensure that these terms are removed from the calculation. For the coincident integration discussed above, the Q integration over s produces terms which are singular at the endpoints of the element, of the form $1/t$ and $1/(1 - t)$. The cancelling contributions appear in the adjacent integrations – for the coincident $\{E_0, E_0\}$ and adjacent $\{E_0, E_{-1}\}$ integrations, it is the $1/t$ term which cancels. However, removing this term is not possible if polar coordinates are employed to the adjacent integration at the outset.

The remedy is simple, isolate the term responsible for producing the singular contribution. The singular point Q_0 corresponds to $s = 1$ for the Q integration over E_{-1}, and to $t = 0$ for P. The only product of shape functions which causes any concern is therefore $s(1 - t) = s - st$, all other combinations are zero at Q_0 and hence effectively balance the singularity in the kernel function. The st term is harmless for the same reason, and thus this term and all other combinations of shape functions are handled by the polar coordinate method mentioned above. This leaves only s times the kernel function, and this is computed using a direct integration over s. The $1/t$ term which appears is seen to cancel with the coincident integration, and consequently dropped.

5
Examples

Two preliminary examples are presented to validate the orthotropic symmetric Galerkin fracture algorithm. Each of these examples involve a single interior crack, one straight (Fig. 3(a)) and one inclined at an angle ϕ with the horizontal (Fig. 3(b)). For both examples, plane stress state is considered. The crack has length $2a = 0.4$, the plate has height $2H = 2.0$ and width $2W = 1.0$. The remote applied traction is denoted by τ_a. Consistent units are used. For the second example (Fig. 3(b)), the angle ϕ has been set equal to 45°. The elastic constants, which correspond to average smeared-out properties of fibreglass, are (Ghandi 1972): $E_1 = 48.26$ GPA, $E_2 = 17.24$ GPA, $\mu_{12} = 6.89$ GPA, and $\nu_{12} = 0.291$.

For the examples, illustrated in Fig. 3, the Cartesian coordinates of the bottom left corner of the plate are $(0, 0)$, and those of the top right corner are (1, 2). The straight crack of Example 1 goes from (0.3, 1.0) to (0.7, 1.0), and the inclined crack of Example 2 goes from (0.3586, 0.8586) to (0.6414, 1.1414). The remote applied traction is $\tau_a = 10$ MPa.

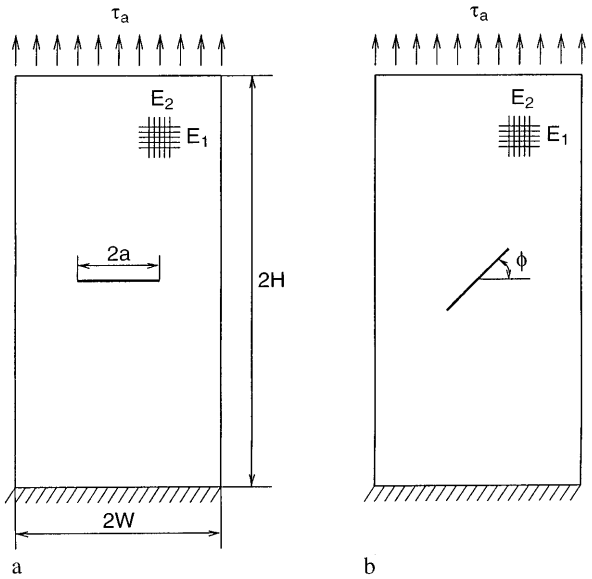

Fig. 3a,b. Geometry and boundary conditions for a central crack in a plane orthotropic plate under remote loading. **a** Example 1: horizontal crack; **b** Example 2: inclined crack

Table 1. Crack Opening Displacement Δu_y for Example 1. The Solution is for half crack, starting at the left crack tip

x	y	SG-BEM $\Delta u_y(\times 10^3)$	FEM $\Delta u_y(\times 10^3)$	$\Delta u_y(\%)$
0.3000	1.000	0.000000	0.000000	0.00
0.325	1.000	0.227131	0.230606	1.51
0.400	1.000	0.391940	0.411062	4.65
0.450	1.000	0.439092	0.460448	4.64
0.500	1.000	0.453433	0.476836	4.91

The above two examples have been solved using the present SG-BEM formulation and compared with the finite element solution provided by the program FRANC: FRacture ANalysis Code (Wawrzynek 1991). The boundary element program does not use special elements at the crack tip, but the finite element program FRANC does. *The parameter chosen for comparison purposes is the displacement discontinuity* $\Delta\mathbf{u}$ *along the crack.*

The FEM mesh for Example 1 has 768 nodes and 266 quadratic elements (six-noded triangles, T6; and eight-noded quadrilaterals, Q8) and the mesh for Example 2 has 790 nodes and 276 elements (T6 and Q8). Figure 4 illustrate the FEM solution for Example 2. Special quarter-point elements are used in the crack tip region, as illustrated by the rosette of finite elements around the crack tips. For the BEM, the outer boundary of the plate has been uniformly discretized with 60 standard linear elements. This discretization coincides with the FEM boundary discretization shown in either Fig. 4; however, the BEM uses linear elements and the FEM uses quadratic ones. Each face of the crack has been discretized by 8 linear boundary elements, with a finer discretization towards the crack tip.

Table 1 shows the results for the crack opening displacement (COD) for the crack of Example 1 (Fig. 3(a)). Because of symmetry, only the results for the left portion of the crack are reported. The last column of this table is computed as

$$\Delta u_\bullet(\%) = \frac{\Delta \mathrm{u}_\bullet(\mathrm{FEM}) - \Delta \mathrm{u}_\bullet(\mathrm{SG\text{-}BEM})}{\Delta \mathrm{u}_\bullet(\mathrm{FEM})} 100\% \qquad (26)$$

The CODs obtained by both the SG-BEM and the FEM are in good agreement, the largest discrepancy being less than 5% . For this problem, the crack sliding displacement (CSD) should be zero (i.e. $\Delta u_x = 0$). The numerical values for both the SG-BEM and the FEM are of the order of 10^{-8} or less, which shows that consistent solutions have been obtained.

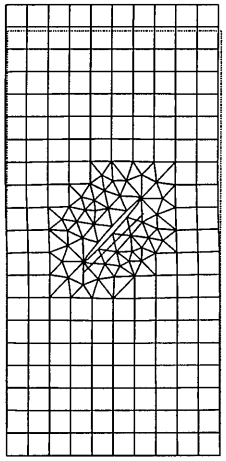

Fig. 4. Finite element solution for an inclined crack in an orthotropic plate under remote tension (790 nodes and 276 quadratic elements); solid line denotes the deformed configuration and the dashed line denotes the original configuration

Table 2 shows the results for the displacement discontinuity $\Delta\mathbf{u} = (\Delta u_x, \Delta u_y)$ for the crack of Example 2 (Fig. 3(b)). As before, the results for Δu_y obtained by both the SG-BEM and the FEM are in good agreement, the largest discrepancy being of 5.07%. However, the results for Δu_x show larger relative discrepancy than the ones for Δu_y (note that the values of $|\Delta u_x|$ are approximately one order of magnitude less than those of $|\Delta u_y|$), especially for the nodes which are the 1/4 point ones in the finite element mesh. These nodes are very close to the crack tip and therefore the results are very sensitive to the numerical discretization. Nevertheless, the actual numerical values for Δu_x obtained by both methods are of comparable magnitudes. Note that the finite element discretization uses quadratic elements (T6 and Q8) and singular crack tip elements; the boundary element discretization uses simpler linear elements everywhere on the mesh. To reduce the difference between the SG-BEM and the FEM results, a much finer boundary element mesh should be used. Moreover, it is expected that the introduction of special singular crack tip elements in the SG-BEM code will significantly improve the results.

Table 2. Displacement discontinuity $\Delta\mathbf{u} = (\Delta u_x, \Delta u_y)$ for Example 2

		SG-BEM		FEM			
x	y	$\Delta u_x(\times 10^4)$	$\Delta u_y(\times 10^3)$	$\Delta u_x(\times 10^4)$	$\Delta u_y(\times 10^3)$	$\Delta u_x(\%)$	$\Delta u_y(\%)$
0.3586	0.8586	0.000000	0.000000	0.000000	0.000000	0.00	0.00
0.3763	0.8763	−0.049903	0.163476	−0.065051	0.164245	23.29	0.47
0.4293	0.9293	−0.105063	0.283705	−0.113276	0.298861	7.25	5.07
0.4646	0.9646	−0.125796	0.318479	−0.139346	0.334257	9.72	4.72
0.5000	1.0000	−0.132743	0.329145	−0.145958	0.345614	9.05	4.77
0.5353	1.0353	−0.125730	0.318613	−0.139309	0.334217	9.75	4.67
0.5707	1.0707	−0.104960	0.283939	−0.113400	0.298794	7.44	4.97
0.6237	1.1237	−0.049838	0.163708	−0.064930	0.164171	23.24	0.28
0.6414	1.1414	0.000000	0.000000	0.000000	0.000000	0.00	0.00

6 Concluding remarks

There are two primary reasons for considering a SG fracture algorithm. First, the Galerkin approximation allows analysis of the hypersingular traction equation with simple standard elements (e.g. linear or quadratic). Differentiable interpolations or non-conforming approximations are much more difficult to work with and computationally expensive. Second, the symmetry provides the needed computational savings to compensate for the additional Galerkin integration. It has been shown herein that crack problems can take special advantage of this symmetry – integrating over the crack can be omitted when constructing the non-crack equations. For the relatively simple 2D problems considered, invoking this feature reduced the computation time by roughly 15%. It is therefore expected that the crossover point where SG becomes more efficient than collocation, already at reasonably sized problems for non-crack geometries, occurs at significantly smaller problem size for fracture.

To further enhance the computational efficiency for three-dimensional problems, it will be necessary to exploit the symmetry of the principal submatrix associated with the crack (i.e., contributions to the crack equations from integrating over the crack). A second issue requiring investigation is the critical area of crack tip approximation. Quarter point elements have recently been employed within a non-conforming dual equation approximation (Sáez et al. 1995), but we are unaware of any special crack tip implementation in conjunction with a Galerkin scheme. In particular, including a special tip element with a SG approximation should be investigated. Finally, a recent result on the form of the displacement in the vicinity of the tip (Gray and Paulino 1997) should be included in the approximation.

Appendix

HBIE Kernels for Orthotropic Elasticity

Tensor $S_{kjL} = U_{kj,L}$

$$S_{111} = \frac{1}{\beta}\left[-\frac{\sqrt{\alpha}_1 A_2^2(Q_1-P_1)}{r_1^2} + \frac{\sqrt{\alpha}_2 A_1^2(Q_1-P_1)}{r_2^2}\right]$$

$$S_{112} = \frac{1}{\beta}\left[-\frac{A_2^2(Q_2-P_2)}{\sqrt{\alpha}_1 r_1^2} + \frac{A_1^2(Q_2-P_2)}{\sqrt{\alpha}_2 r_2^2}\right]$$

$$S_{121} = \frac{1}{\beta}\left[-\frac{(Q_2-P_2)A_2A_1}{\sqrt{\alpha}_1 r_1^2} + \frac{(Q_2-P_2)A_2A_1}{\sqrt{\alpha}_2 r_2^2}\right]$$

$$S_{122} = \frac{1}{\beta}\left[\frac{(Q_1-P_1)A_2A_1}{\sqrt{\alpha}_1 r_1^2} - \frac{(Q_1-P_1)A_2A_1}{\sqrt{\alpha}_2 r_2^2}\right]$$

$$S_{211} = S_{121}$$

$$S_{212} = S_{122}$$

$$S_{221} = \frac{1}{\beta}\left[\frac{A_1^2(Q_1-P_1)}{\sqrt{\alpha}_1 r_1^2} - \frac{A_2^2(Q_1-P_1)}{\sqrt{\alpha}_2 r_2^2}\right]$$

$$S_{222} = \frac{1}{\beta}\left[\frac{A_1^2(Q_2-P_2)}{\alpha_1^{3/2} r_1^2} - \frac{A_2^2(Q_2-P_2)}{\alpha_2^{3/2} r_2^2}\right]$$

Tensor $W_{kjL} = T_{kj,L}$

$$W_{111} = \frac{1}{\beta}\left\{\frac{n_x A_2}{\sqrt{\alpha}_1 r_1^2} - \frac{n_x A_1}{\sqrt{\alpha}_2 r_2^2} + 2\mathbf{n}\cdot\mathbf{R}(Q_1-P_1)\left[\frac{A_1}{\sqrt{\alpha}_2 r_2^4} - \frac{A_2}{\sqrt{\alpha}_1 r_1^4}\right]\right\}$$

$$W_{112} = \frac{1}{\beta}\left\{\frac{n_y A_2}{\sqrt{\alpha}_1 r_1^2} - \frac{n_y A_1}{\sqrt{\alpha}_2 r_2^2} + 2\mathbf{n}\cdot\mathbf{R}(Q_2-P_2)\left[\frac{A_1}{\alpha_2^{3/2} r_2^4} - \frac{A_2}{\alpha_1^{3/2} r_1^4}\right]\right\}$$

$$W_{121} = \frac{1}{\beta}\left\{-\frac{\sqrt{\alpha}_1 n_y A_2}{r_1^2} + \frac{\sqrt{\alpha}_2 n_y A_1}{r_2^2} + 2(Q_1-P_1)\left[-\frac{F_2A_1}{r_2^4} + \frac{F_1A_2}{r_1^4}\right]\right\}$$

$$W_{122} = \frac{1}{\beta}\left\{\frac{n_x A_2}{\sqrt{\alpha}_1 r_1^2} - \frac{n_x A_1}{\sqrt{\alpha}_2 r_2^2} + 2(Q_2-P_2)\left[-\frac{F_2A_1}{\alpha_2 r_2^4} + \frac{F_1A_2}{\alpha_1 r_1^4}\right]\right\}$$

$$W_{211} = \frac{1}{\beta}\left\{-\frac{n_y A_1}{\sqrt{\alpha}_1 r_1^2} + \frac{n_y A_2}{\sqrt{\alpha}_2 r_2^2} + 2(Q_1-P_1)\left[\frac{F_1A_1}{\alpha_1 r_1^4} - \frac{F_2A_2}{\alpha_2 r_2^4}\right]\right\}$$

$$W_{212} = \frac{1}{\beta}\left\{\frac{n_x A_1}{\alpha_1^{3/2} r_1^2} - \frac{n_x A_2}{\alpha_2^{3/2} r_2^2} + 2(Q_2-P_2)\left[\frac{F_1A_1}{\alpha_1^2 r_1^4} - \frac{F_2A_2}{\alpha_2^2 r_2^4}\right]\right\}$$

$$W_{221} = \frac{1}{\beta}\left\{-\frac{n_x A_1}{\sqrt{\alpha}_1 r_1^2} + \frac{n_x A_2}{\sqrt{\alpha}_2 r_2^2} + 2\mathbf{n}\cdot\mathbf{R}(Q_1-P_1)\left[\frac{A_1}{\sqrt{\alpha}_1 r_1^4} - \frac{A_2}{\sqrt{\alpha}_2 r_2^4}\right]\right\}$$

$$W_{222} = \frac{1}{\beta}\left\{-\frac{n_y A_1}{\sqrt{\alpha}_1 r_1^2} + \frac{n_y A_2}{\sqrt{\alpha}_2 r_2^2} + 2\mathbf{n}\cdot\mathbf{R}(Q_2-P_2)\left[\frac{A_1}{\alpha_1^{3/2} r_1^4} - \frac{A_2}{\alpha_2^{3/2} r_2^4}\right]\right\}$$

The parameters $F_i (i = 1, 2)$ are

$$F_1 = \sqrt{\alpha}_1 n_y(Q_1-P_1) - \frac{n_x(Q_2-P_2)}{\sqrt{\alpha}_1} \quad ,$$

$$F_2 = \sqrt{\alpha}_2 n_y(Q_1-P_1) - \frac{n_x(Q_2-P_2)}{\sqrt{\alpha}_2} \quad ,$$

and

$$\mathbf{n}\cdot\mathbf{R} = n_x(Q_1-P_1) + n_y(Q_2-P_2) \quad .$$

References

Blandford, G. E.; Ingraffea, A. R.; Liggett, J. A. (1981): Two-dimensional stress intensity factor computations using the boundary element method. Int. J. Num. Meth. Eng. 17, 387–404

Bonnet, M.; Bui, H. D. (1993): Regularization of the displacement and traction BIE for 3D elastodynamics using indirect methods. In: Kane, J. H.; Maier, G.; Tosaka, N.; Atluri, S. N. (eds.): Advances in Boundary Element Techniques, Chapter 1, pp. 1–29. Berlin, Heidelberg: Springer-Verlag

Chang, C.; Mear, M. E. (1995): A boundary element method for two dimensional linear elastic fracture analysis. Int. J. Fract. 74, 219–251

Crouch, S. L.; Starfield, A. M. (1983): Boundary Element Methods in Solid Mechanics. London: George Allen & Unwin

Cruse, T. A. (1988): Boundary Element Analysis in Computational Fracture Mechanics. Dordrecht: Kluwer Academic Publishers

Ghandi, K. R. (1972): Analysis of an inclined crack centrally placed in an orthotropic rectangular plate. J. Strain Analysis 7, 157–162

Gray L. J. (1991): Evaluation of hypersingular integrals in the boundary element method. Math. Comput. Model. 15 (3–5), 165–174

Gray, L. J. (1993): Symbolic computation of hypersingular boundary integrals. In: Kane, J. H.; Maier, G.; Tosaka, N.; Atluri, S.N. (eds.): Advances in Boundary Element Techniques. Chapter 8, pp. 157–172. Berlin, Heidelberg: Springer-Verlag

Gray, L. J.; Paulino, G. H. (1997): Crack tip interpolation, revisited. SIAM J. Appl. Math. (in press)

Gray, L. J.; Martha, L. F.; Ingraffea, A. R. (1990): Hypersingular integrals in boundary element fracture analysis. Int. J. Num. Meth. Eng. 29, 1135–1158

Gray, L. J.; Balakrishna, C.; Kane J. H. (1995): Symmetric Galerkin boundary integral fracture analysis. Eng. Anal. Bound. Elements 15, 103–109

Green, A. E. (1943): A note on stress systems in aeolotropic materials. Philosoph. Mag. 34, 416–418

Guimarães, S.; Telles, J. C. F. (1994): On the hyper-singular boundary-element formulation for fracture-mechanics applications. Eng. Anal. Bound. Elements 13 (4), 353–363

Hall, W. S.; Hibbs, T. T. (1988): The treatment of singularities and the application of the Overhauser $C^{(1)}$ continuous quadrilateral boundary element to three dimensional elastostatics. In: Cruse, T. A. (ed.): Advanced Boundary Element Methods, volume 16, pp. 135–144. Berlin, Heidelberg: Springer-Verlag

Hartmann, F.; Katz, C.; Protopsaltis, B. (1985): Boundary elements and symmetry. Ingenieur-Archive 55 (6), 440–449

Hong, H.; Chen, J. (1988): Derivations of integral equations of elasticity. J. Eng. Mech. 114, 1028–1044

Krishnasami, G.; Rizzo, F. J.; Rudolphi, T. J. (1992): Hypersingular Boundary integral Equations: Their Occurrence, interpretation, Regularization and Computation. In: Banerjee, P. K.; Kobayashi, S. (eds.): Developments in Boundary Element Methods volume 7, chapter 6, pp. 207–252. London and New York: Elsevier Applied Science

Lutz, E. D.; Gray, L. J. (1993): Analytic Evaluation of Singular Boundary Integrals without CPV. Commun. Num. Meth. Eng. 9 (11), 909–915

Maier, G.; Polizzotto, C. (1987): A Galerkin approach to boundary element elastoplastic analysis. Comput. Meth. Appl. Mech. Eng. 60, 175–194

Martin, P. A.; Rizzo, F. J. (1996): Hypersingular integrals: how smooth must the density be? Int. J. Num. Meth. Eng. 39, 687–704

Paulino, G. H. (1995): Novel Formulations of the Boundary Element Method for Fracture Mechanics and Error Estimation. Ph.D. dissertation, Cornell University, Ithaca, New York, USA

Paulino, G. H.; Saif, M. T. A.; Mukherjee, S. (1993): A finite elastic body with a curved crack loaded in anti-plane shear. Int. J. Solids Struct. 30 (8), 1015–1037

Rizzo, F. J.; Shippy, D. J. (1970): A method for stress determination in plane anisotropic elastic bodies. J. Comp. Mat. 4, 36–61

Rizzo, F. J.; Shippy, D. J.; Rezayat, M. (1985): A boundary integral equation method for radiation and scattering of elastic waves in three dimensions. Int. J. Num. Meth. Eng. 21, 115–129

Rudolphi, T. J. (1990): Higher order elements and element enhancement by combined regular and hypersingular boundary integral equations. In: Annigeri, B. S.; Tseng, K. (eds.): Boundary Element Methods in Engineering, pp. 448–455, Berlin, Heidelberg: Springer-Verlag

Sáez, A.; Gallego, R.; Dominguez, J. (1995): Hypersingular quarter-point boundary elements for crack problems. Int. J. Num. Meth. Eng. 38 (10), 1681–1701

Selcuk, S.; Hurd, D. S.; Crouch, S. L.; Gerberich, W. W. (1994): Prediction of interfacial crack path: a direct boundary integral approach and experimental study. Int. J. Fract. 67 (1), 1–20

Sirtori, S.; Maier, G.; Novati, G; Miccoli, S. (1992): A Galerkin symmetric boundary-element method in elasticity: formulation and implementation. Int. J. Num. Meth. Eng. 35, 255–282

Tan, C. L.; Gao, Y. L. (1992): Boundary integral equation fracture mechanics analysis of plane orthotropic bodies. Int. J. Fract. 53, 343–365

Walters, H. G.; Ortiz, J. C.; Gipson, G. S.; Brewer III, J. A. (1988): Overhauser boundary elements in potential theory and linear elastostatics. In: Cruse, T. A. (ed.): Advanced Boundary Element Methods, volume 16, pp. 459–464. Berlin, Heidelberg: Springer-Verlag

Watson, J. O. (1986): Hermitian cubic and singular elements for plane strain. In: Banerjee, P. K.; Watson, J. O. (eds): Developments in Boundary Element Methods, volume 4, chapter 1, pp. 1–28. London and New York: Elsevier Applied Science

Wawrzynek, P. A. (1991): Discrete Modeling of Crack Propagation: Theoretical Aspects and Implementation Issues in Two and Three Dimensions. Ph.D. dissertation, Cornell University, Ithaca, New York, USA